Detecting interannual variation in deciduous broadleaf forest phenology using Landsat TM/ETM + data

Eli K. Melaas *, Mark A. Friedl, Zhe Zhu

Department of Earth and Environment, Boston University, 675 Commonwealth Avenue, Boston, MA 02215, United States

ABSTRACT

Observations of vegetation phenology provide valuable information regarding ecosystem responses to climate variability and change. Phenology is also a first-order control on terrestrial carbon and energy budgets, and remotely sensed observations of phenology are often used to parameterize seasonal vegetation dynamics in ecosystem models. Current land surface phenology products are only available at moderate spatial resolution and possess considerable uncertainty. Higher resolution products that resolve finer spatial detail are therefore needed. A need also exists for data sets and methods that link ground-based observations of phenology to moderate resolution land surface phenology products. Data from the Landsat TM and ETM + sensors have the potential to meet these needs, but have been largely unexplored by the phenology research community. In this paper we present a method for characterizing both long-term average and interannual dynamics in the phenology of temperate deciduous broadleaf forests using multi-decadal time series of Landsat TM/ETM + images. Results show that spring and autumn phenological transition dates estimated from Landsat data agree closely with in-situ measurements of phenology collected at the Harvard Forest in central Massachusetts, and that Landsat-derived estimates for the start and end of the growing season in Southern New England varied by as much as 4 weeks over the 30-year record of Landsat images. Application of this method over larger scales has the potential to provide valuable information related to landscape-scale patterns and long term dynamics in phenology, and for bridging the gap between in-situ phenological measurements collected at local scales and land surface phenology metrics derived from moderate spatial resolution of instruments such as MODIS and AVHRR.

© 2013 Elsevier Inc. All rights reserved.

1. Introduction

In most temperate ecosystems, forest canopy processes related to leaf development and senescence are strongly controlled by air temperature (Chuine et al., 2010; Delpierre et al., 2009). As a result, spatio-temporal patterns in phenology are widely viewed to be important indicators of climate change (Cleland et al., 2007). Growing season dynamics are also tightly coupled with biosphere–atmosphere interactions (Churkina et al., 2005; Richardson et al., 2009), and accurate representation of phenology is therefore important in land surface models (Richardson et al., 2012). To support studies of how ecosystems are responding to climate change and reduce uncertainty in terrestrial energy and carbon budgets, better datasets characterizing the response of vegetation phenology to variations in climate are required (Morisette et al., 2009).

Phenological observations are traditionally collected using two main approaches: (1) surface observation networks (Schwartz et al., 2012), and (2) high frequency, coarse spatial resolution satellite remote sensing (e.g., Jonsson & Eklundh, 2002). Surface observations provide detailed information related to the timing of leaf development and flowering phenology for individual plants. However, the utility of such data for large-scale monitoring and model development is constrained by data availability, the limited spatial extent of available samples, and biases inherent to methods used to characterize the phenology of plants (Cleland et al., 2007).

Remotely sensed data collected by instruments such as the Advanced Very High Resolution Radiometer (AVHRR) and the Moderate Resolution Imaging Spectroradiometer (MODIS) provide near-daily global observations of vegetation dynamics at 250 m to 8 km spatial resolution. Exploiting this high frequency acquisition strategy, numerous remote sensing products and algorithms have been developed over the past two decades that use time series of vegetation indices such as the normalized difference vegetation index (NDVI) to track seasonal plant activity (e.g., de Beurs & Henebry, 2010; Ganguly et al., 2010; Jonsson & Eklundh, 2002; Moulin et al., 1997; Reed et al., 1994; White et al., 1997). These products and algorithms have been shown to successfully capture regional-to-global phenological patterns. However, they are less reliable at local scales and in areas with heterogeneous land cover where remotely sensed measurements

* Corresponding author at: 675 Commonwealth Ave. Room 132, Boston University, Boston, MA 02215, United States. Tel.: +1 248 343 9278; fax: +1 617 353 8399.
E-mail addresses: emelaas@bu.edu (E.K. Melaas), friedl@bu.edu (M.A. Friedl), zhuzhe@bu.edu (Z. Zhu).

reflect mixtures of land cover types, plant species, and plant functional types (Badeck et al., 2004; Liang et al., 2011).

Bridging the gap between ground observations and moderate resolution remote sensing approaches, Fisher et al. (2006) used a time series of 57 Landsat images to generate a map of long-term average spring phenology across Southeastern New England. At 30 m spatial resolution, this map yielded substantial information related to spatial patterns and sources of local variability in leaf phenology that are not observable from lower spatial resolution instruments such as MODIS. Landsat spatial resolution also supports analyses at regional scales (1 scene ~31,000 km²) and allows factors that control phenology over relatively short spatial scales to be explored (e.g., topography, land use and urban heat islands, and coastal effects). However, because Landsat image acquisitions are relatively infrequent compared to moderate resolution sensors such as MODIS, Landsat-based characterization of phenology at annual time scale using conventional methodologies such as those described by Jonsson and Eklundh (2002) or Zhang et al. (2003) is challenging. Some efforts have addressed this using data fusion algorithms that blend MODIS with Landsat data (e.g., Walker et al., 2012). However, retrieval of phenological information from such fused data sets is complicated by land cover heterogeneity below the spatial resolution of MODIS and uncertainty introduced by the data fusion algorithm (Tan et al., 2006; Zhu et al., 2010).

In this paper we extend the work of Fisher et al. (2006) to develop an algorithm that uses time series of Landsat images to characterize both long-term average and interannual variability in vegetation phenology. Our analysis was made possible by the opening of the Landsat archive (Woodcock et al., 2008), which provides new opportunities for higher spatial resolution analyses of phenology. We exploit this potential using a 30-year time series of Landsat images to develop and test a simple algorithm that efficiently and accurately estimates both long-term average phenology and annual spring and autumn transition dates in temperate deciduous forests.

2. Materials and methods

2.1. Landsat data

We used all available TM/ETM + L1T images from 1982 to 2011 with cloud cover less than 80% (a total of 541 images; Fig. 1) for a Landsat scene centered over southern New England (Path 12 Row 31; Fig. 2). The land area in this scene encompasses a mix of land cover types characteristic of Southern New England, including substantial areas of deciduous broadleaf forest. The northeast quadrant of this scene contains the Harvard Forest Long Term Ecological Reserve site (http://harvardforest.fas.harvard.edu/), where more than 20 years of in-situ vegetation phenology measurements have been collected and are available for comparison with time series of Landsat measurements. To reduce atmospheric effects, DN values from each image were converted to units of surface reflectance using the Landsat Ecosystem Disturbance Adaptive Processing System (LEDAPS) atmosphere correction tool (Vermote et al., 1997; Masek et al., 2008), which uses the MODIS/6S radiative transfer model. Clouds, cloud shadows, and snow were screened using an algorithm that has recently been developed at Boston University called Fmask (Zhu & Woodcock, 2012).

2.2. Phenology algorithm

Most satellite-based algorithms for monitoring phenology use either the Normalized Difference Vegetation Index (NDVI) or the Enhanced Vegetation Index (EVI). While both of these indices capture seasonal changes in vegetation properties, the EVI provides a larger dynamic range than the NDVI over vegetation with high leaf area (Huete et al., 2002). Here we used the EVI to develop an algorithm that detects spatio-temporal patterns in phenology using two main steps.

The first step in our algorithm estimates a model of long-term average annual phenology as a function of day of year (DOY) using all cloud-free
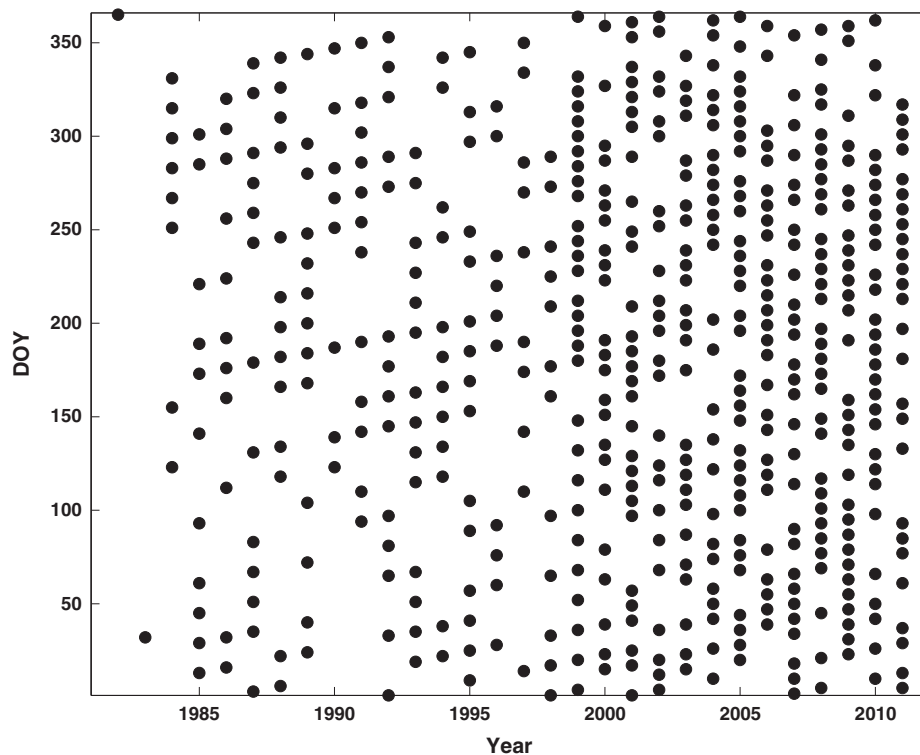

Fig. 1. Schematic showing the number and timing of Landsat TM/ETM + images used in the study. Each point represents a single Landsat image. Note how the density of observations increases after the launch of Landsat 7.
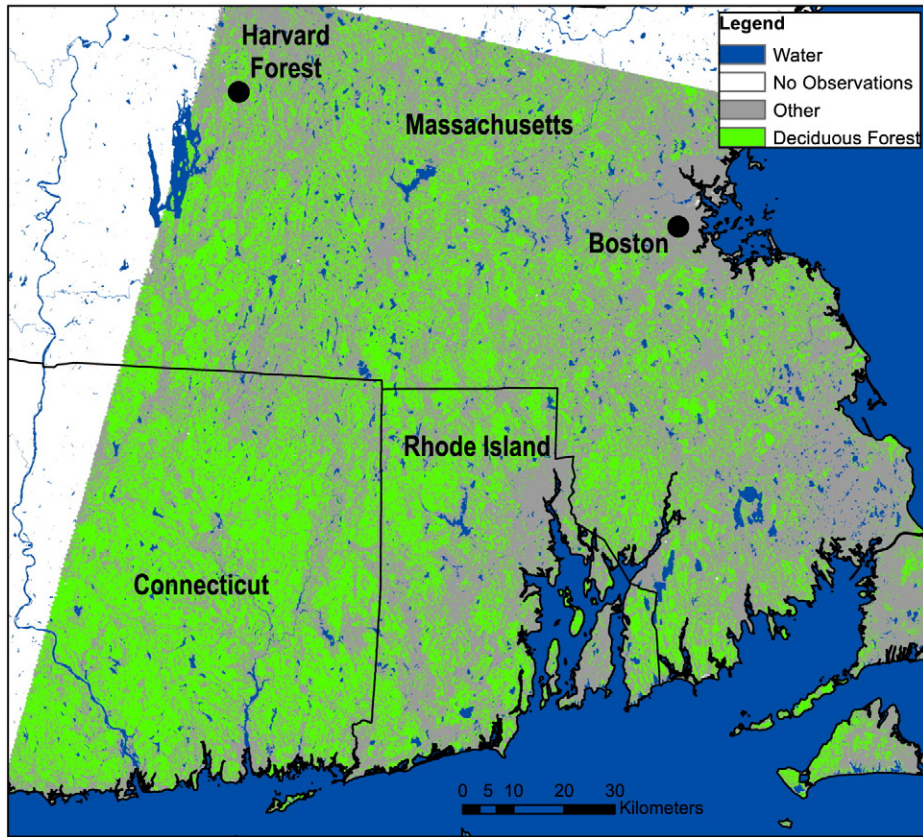
Fig. 2. Study region located in southern New England. Green pixels were classified as deciduous forest based on the method described in Section 2.3, and pixels labeled as "Other" were classified as non-deciduous forest. Pixels labeled as "No Observations" either fall outside the Landsat scene's spatial extent or have ≤100 cloud-free observations. Water areas were mapped using to the 2006 National Land Cover Dataset (Xian et al., 2009).
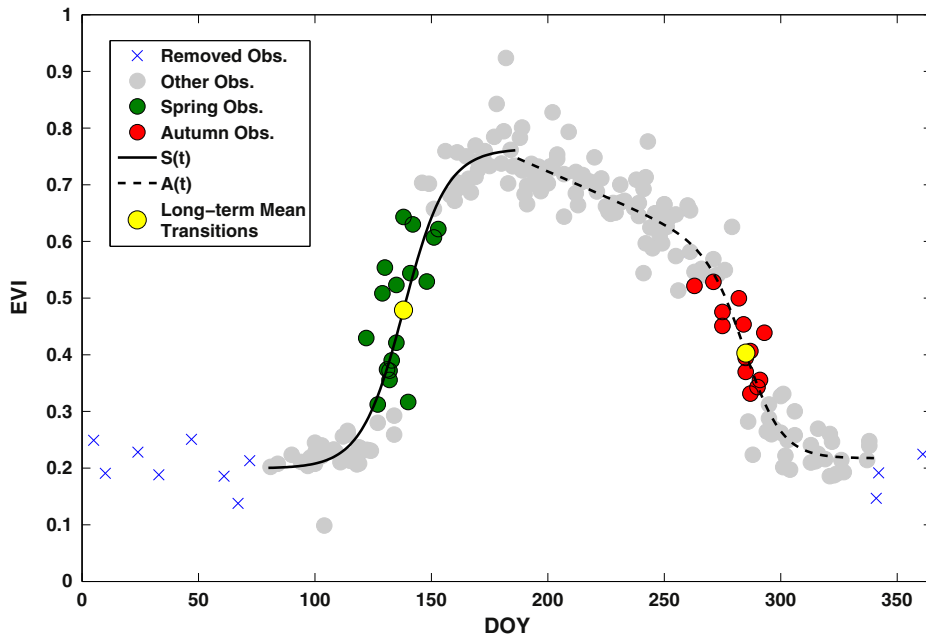

Fig. 3. An example of multi-year phenology for one Landsat pixel located at Harvard Forest, MA. Green and red dots identify observations used to estimate interannual anomalies in transition dates for spring and autumn, respectively. Spring and autumn anomalies are calculated as the difference between the date of each observation and the date where the logistic curve ($S(t)$ for spring; $A(t)$ for autumn) reaches the corresponding EVI value. Transition dates for each year are then estimated as the sum of the long-term mean transition date (yellow dots) and the estimated anomaly. Points identified with x's are outside the date range of the analysis.

EVI values at each pixel (Fig. 3). To do this, we fit separate spring and autumn logistic functions to EVI time series at each pixel, and use these functions to estimate long-term average spring onset and autumn offset dates (p_s and p_a, respectively). Spring greenup was modeled using a 4 parameter logistic function (Zhang et al., 2003):

$$S(t) = m_1 + \frac{m_2}{1 + e^{-m_3(t-m_4)}} \tag{1}$$

where t is time (expressed as DOY), m_1 is the pre-greenup background EVI, $m_1 + m_2$ is the maximum EVI, and m_3 and m_4 control the slope and phase, respectively. Long-term mean spring onset dates were estimated as the DOY corresponding to when the first derivative of $S(t)$ is maximum, which coincides with the most stable and well-constrained portion of functions estimated using Eq. (1). Uncertainty in logistic function fits is therefore lower during this period relative to other portions of the curve.

As described by Elmore et al. (2012), a gradual decrease in EVI ("greendown") is commonly observed during the summer in many deciduous broadleaf forests. As a result, Eq. (1) sometimes provides a sub-optimal representation of autumn dynamics in EVI. To account for this, we modeled EVI dynamics during the mid-summer and autumn using the 5 parameter logistic function proposed by Elmore et al. (2012):

$$A(t) = n_1 + \frac{n_2 t + n_3}{1 + e^{n_4(n_5-t)}} \tag{2}$$

where n_1 is the leaf-off season background EVI, n_2 and n_3 control the trajectory of EVI during the mid-growing season, and n_4 and n_5 control the slope and phase, respectively. Following Elmore et al. (2012) autumn offset dates were estimated using the value of n_5 in Eq. (2), which corresponds to the DOY when the derivative of Eq. (2) is maximum. To optimize the logistic model fits in both spring and fall, nonlinear regressions were estimated using the Levenberg–Marquardt algorithm (Levenberg, 1944).

Estimation of coefficients for Eqs. (1) and (2) is sensitive to the range of dates and density of EVI observations. To determine the best date for transitioning from $S(t)$ to $A(t)$, we compute the slope of EVI for moving windows composed of 21 observations starting on DOY 90. The DOY corresponding to the mid-point for the first window detected to have a negative slope was identified as the transition point between the spring and autumn logistic functions. Observations before DOY 80 and after DOY 340 were excluded during the early spring and late autumn periods, respectively, and pixels with fewer than 100 cloud-free observations were excluded from the analysis. However, because Eqs. (1) and (2) are estimated using a different number of observations at each pixel, it was important to evaluate the sensitivity of our approach to variation in the number of EVI observations at each pixel. To do this, we generated 2500 unique EVI time series with n ranging from 100 to 288 by randomly sampling from the pixel with the largest number of cloud free observations in the scene ($n = 288$). We then estimated spring and autumn logistic models for each time series and used the results to characterize how variation in the number of samples affects uncertainty in our results.

In the second step of our algorithm, we use the estimated long-term mean phenology models at each pixel to quantify interannual variability in phenology during both spring and autumn. To accomplish this, we examined all observations acquired within ± 20 days of the long-term mean transition dates whose EVI values met the following criteria for spring (a and b) and autumn (a and c):

a: $EVI \geq min[F(t)] + 0.2 \times (max[F(t)] - min[F(t)])$
b: $EVI \leq max[F(t)] + 0.2 \times (max[F(t)] - min[F(t)])$
c: $EVI \geq max[F(t)] - 0.4 \times (max[F(t)] - min[F(t)])$

where $F(t)$ is Eq. (1) for spring observations and Eq. (2) for autumn observations. These criteria are designed to include observations acquired during the most stable portion of each logistic curve. For each observation that meets these criteria, we compute the deviation between the DOY on which the observation was acquired and the DOY corresponding to the same EVI value for the logistic function(s) fit across all years (i.e., in Fig. 3, the horizontal deviation between each selected EVI value and the fitted logistic function). This deviation provides an estimate of the annual anomaly in the timing of spring onset and autumn offset dates relative to the long-term average. If more than one observation from the same year meet the criteria described above, we use the mean deviation across all qualifying observations. The spring onset and autumn offset dates for each year are then computed by adding the estimated annual deviation to the mean transition date; i.e. $p_s + \Delta t$ and $p_a + \Delta t$, where p_s and p_a are the long term average spring onset and fall offset dates, respectively, and Δt is the annual anomaly in spring or fall, as defined above.

2.3. Deciduous forest stratification

The method we describe above is designed to characterize both long-term average and interannual dynamics in the phenology of deciduous broadleaf forests. To do this, our algorithm exploits the large amplitude in EVI at each pixel that results from the seasonal emergence and loss of leaves. Before applying our method, we exploited this property to distinguish deciduous forest from other land cover types (e.g., Donohue et al., 2009; Fisher et al., 2006). Specifically, using the long-term lower (m_1) and upper asymptote ($m_1 + m_2$) of EVI derived from the estimated spring logistic function, we classified pixels as deciduous forest if the lower asymptote of EVI was between 0.1 and 0.25 and the upper asymptote was between 0.6 and 0.9. Both thresholds were chosen based on comparison of EVI time series with high-resolution imagery acquired during the leaf-off season (Fig. 4a). To exclude pixels affected by land cover change, we computed the 95th percentile of EVI values at each pixel identified as deciduous forest for two periods (1982–2005 and 2006–2011). Pixels for which the 95th percentile in EVI decreased by more than 0.2 between these two periods were assumed to have experienced some type of land cover change, and we excluded from further analysis.

2.4. Algorithm assessment

To assess the ability of our algorithm to capture interannual variability in spring and autumn phenology, we used a 22-year time series of in-situ observations collected at the Harvard Forest in Petersham, MA from 1990 to 2011. Tree species composition at Harvard Forest is representative of temperate forests in southern New England and is dominated by red oak (*Quercus rubra*, 36% of basal area), red maple (*Acer rubra*, 22% of basal area) and yellow birch (*Betula allaghaniensis*, 14% of basal area), with smaller quantities of other hardwoods and some conifer, primarily eastern hemlock (*Tsuga canadensis*) (Richardson et al., 2009). Stem density in the forest is approximately 660 stems ha^{-1}, which corresponds to roughly 60 stems per Landsat pixel (Moore et al., 1996), and green leaf area index in deciduous stands reaches a seasonal maximum of ~5.5 (Urbanski et al., 2007). The in-situ measurements we use here consist of visual observations of leaf length and coloration collected during spring and autumn (respectively) for at least three individuals of eleven tree species at 3–7 day intervals (O'Keefe, 2000).

Spring and autumn transition dates estimated by our Landsat-based method were compared against ground observations using a 60 × 60 pixel window (~3.2 km^2) centered over the area on the ground where in-situ measurements were collected. To perform this comparison, we used the basal area proportions for each of the three dominant species identified above to compute site-wide weighted averages for leaf length in spring and leaf coloration in fall on each ground observation date. We then compared spring onset and autumn offset dates estimated from Landsat data with the resulting time series of leaf length and leaf color measurements at 5% intervals from 5% to
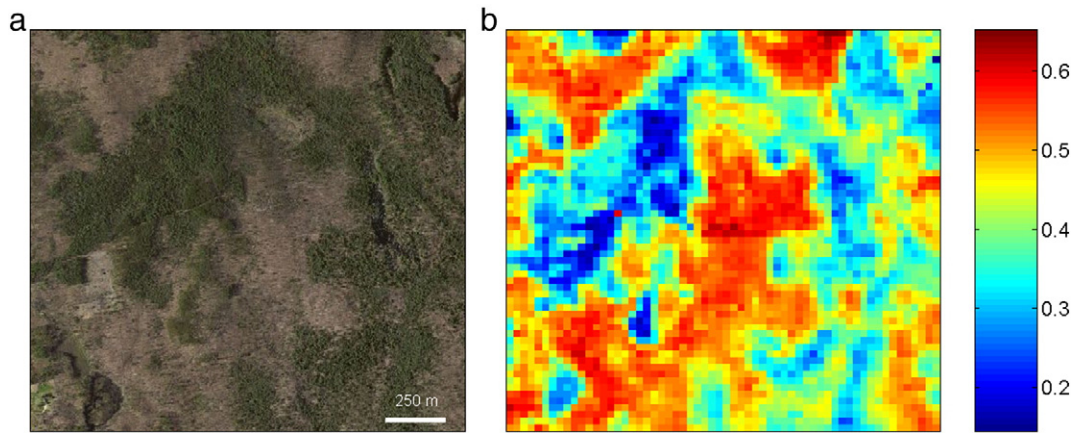
Fig. 4. (a) Aerial photo of Harvard Forest during the leaf-off season. Light brown areas are mainly deciduous forest and green areas are evergreen forests; (b) corresponding annual EVI amplitude across a 60×60 pixel window (3.24 km^2) covering the same area. Note that pixels with high amplitude (> 0.45) correspond to areas with deciduous forest.

95%. This analysis indicated that spring onset and fall offset dates were most strongly related to the DOY when leaves reached 25% of their maximum length and when 90% of leaves reached peak coloration, respectively (Fig. 5). In the results below, these two metrics are a basis for assessing results from Landsat.

3. Results

Fig. 3 plots Landsat EVI values versus DOY along with estimated spring and fall logistic fits for a representative deciduous forest pixel at Harvard Forest. Both spring and autumn logistic curves realistically capture the average timing of increase and decrease in EVI using the algorithm described in Section 2.2. The yellow dots in Fig. 3 identify the long-term mean spring onset (DOY 138 = May 18) and autumn offset dates (DOY 285 = Oct 12). The green and red dots identify EVI observations that meet the criteria defined in Section 2.2 and were used to calculate annual onset and offset dates at this pixel. Observations located to the left of the fitted logistic functions indicate that spring greenup or autumn offset occurred earlier than average, while data points

located to the right of the fitted functions indicate later development or senescence of leaves in the spring and autumn, respectively.

Fig. 4a presents an aerial photograph of Harvard Forest (obtained from Bing Maps: www.bing.com/maps) that was acquired during the leaf-off season when evergreen and deciduous forest areas are distinguishable from each another. Fig. 4b shows the long-term average amplitude in EVI estimated from the fitted spring logistic curve (i.e., m_2 in Eq. (1) at each Landsat pixel in a 60×60 window co-located with the image in Fig. 4a. Red and orange colored areas in this figure identify deciduous broadleaf stands (larger amplitude), while blue colored areas have low EVI amplitude and correspond to evergreen needleleaf stands or other non-deciduous land cover types. Yellow regions have moderate amplitudes that are characteristic of mixed forests. Based on the stratification procedure described in Section 2.3, 37% of pixels in the 60×60 pixel window are deciduous broadleaf forest.

Fig. 6 shows EVI time series for 3 pixels that span the range of cloud-free observations in the scene, along with a histogram showing the distribution of cloud free observations between DOY 80 and 340 at each pixel across the entire scene. The median number of cloud
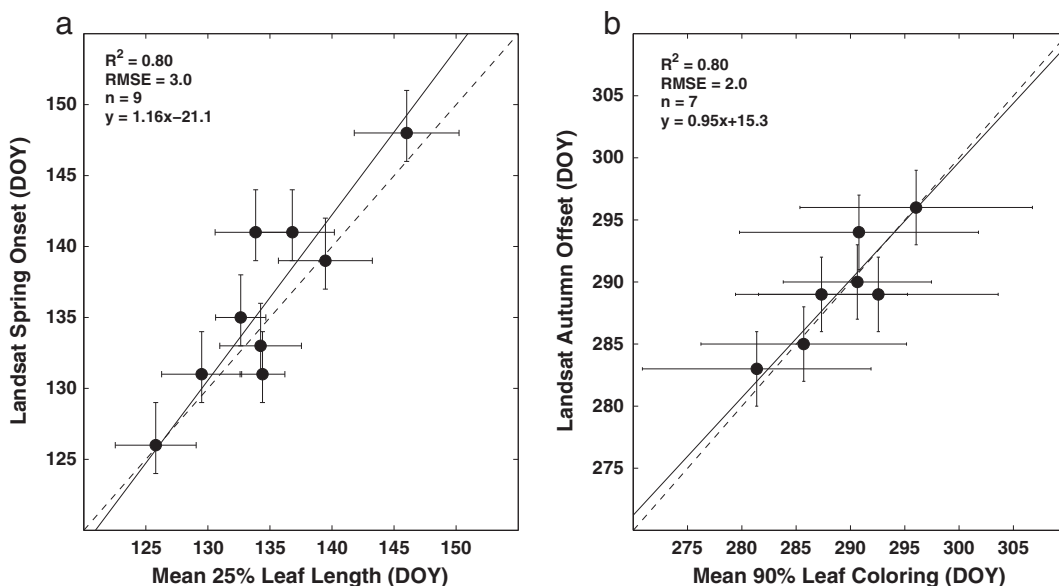

Fig. 5. (a) Landsat-derived spring onset date versus the mean date when leaf length of common deciduous tree species reached 25% of maximum for one pixel at Harvard Forest; (b) Landsat-derived autumn offset versus the mean date when leaves of deciduous species reached 90% coloring. Vertical error bars represent 95% confidence intervals for Landsat estimated transition dates. Horizontal bars show ± 1 standard deviation for spring and autumn in-situ phenology metrics. Dashed lines are 1:1.

free EVI values was 240, the maximum was 288, and the vast majority of pixels had more than 200 cloud free observations available. Fig. 7 presents results showing the sensitivity of logistic function coefficients to variation in the number of samples at each pixel. These results show that the slope and phase coefficients for both spring and autumn logistic functions are relatively insensitive to the number of EVI time series observations at each pixel, at least for the range of time series considered here. Specifically, 95% confidence intervals for the slope coefficient in spring and fall were ±0.029 and ±0.023 (respectively), which translate into uncertainties in spring onset and autumn offset of ±1.0 days. Similarly, 95% confidence intervals for the phase coefficient were ±2.0 days for spring and ±2.3 days for autumn. Uncertainty in model coefficients gradually increases as the number of observations decreases below 200. However, as we describe above, the vast majority of pixels in the Landsat scene considered here have at least 200 cloud-free observations.

Landsat-based estimates of annual spring and autumn transition dates correspond closely to the timing of in-situ observations at Harvard Forest. Fig. 8 plots the RMSE and R^2 between ground observations and Landsat-derived estimates of spring phenology at each deciduous forest pixel in Fig. 4b, which corresponds to the area within Harvard Forest where the in-situ measurements were collected. Agreement between ground observations and Landsat retrievals is uniformly high over the window: average RMSE and R^2 values in spring were 3.4 ± 0.8 days and 0.79 ± 0.10, respectively. Autumn transition dates estimated from Landsat (not shown) were also highly correlated with observed dates (RMSE $= 4.7 \pm 1.8$; $R^2 = 0.64 \pm 0.21$). Spatial variation in Fig. 8a and b is controlled by several factors including pixel-to-pixel variation in forest phenology and uncertainty in the species composition, noise inherent to the Landsat EVI data, and

uncertainty in the algorithm itself. Note that depending on the density of EVI data in the spring and fall of any year (which varies across pixels because of cloud cover and missing data introduced by the ETM + scan line corrector problem), it is not possible to estimate onset and offset dates in all years. To illustrate, Fig. 9 shows the number of spring and autumn retrievals (out of a possible 30 years) at each deciduous forest pixel. On average, the algorithm was able to estimate spring onset and autumn offset dates in 10 and 9 years, respectively, out of thirty.

4. Discussion

Observations of phenology have been made using remote sensing for over three decades. Indeed, Multispectral Scanner System data was used to monitor crop phenology early in the Landsat program (e.g., Badhwar, 1980). Recently, however, the vast majority of remote sensing applications related to phenology have used coarse or moderate spatial resolution data from sensors such as the AVHRR or MODIS (White et al., 2009; Zhang et al., 2003). Relative to these instruments, higher spatial resolution sensors such as the Landsat TM and ETM + acquire imagery at much less frequent intervals and have been largely ignored as a source of data for phenological studies. The availability of long and dense time series of Landsat data, especially in regions of the world such as North America where the Landsat archive is densely populated, provides new opportunities to exploit Landsat data in regional (and potentially continental) studies of vegetation phenology.

In this paper, we present and test a new method for detecting long-term average and interannual variation in spring and autumn phenology of temperate deciduous broadleaf forests using Landsat data. The algorithm is simple, computationally efficient, and based
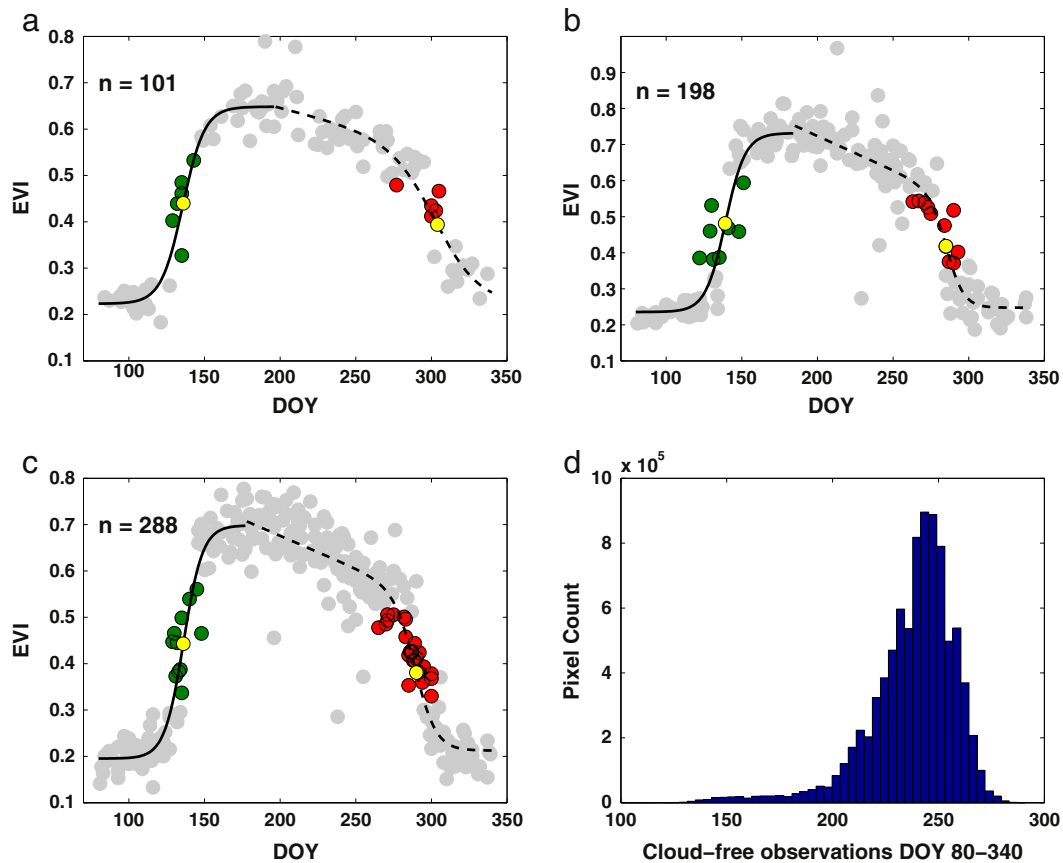

Fig. 6. Multi-year phenological variability for Landsat pixels with the (a) minimum, (b) median, and (c) maximum numbers of cloud-free observations between DOY 80-340 in the Landsat scene used in this study. The number of EVI observations (n) is displayed in the upper left corner of each plot; (d) histogram showing the number of cloud-free observations for all deciduous forest pixels across the entire Landsat scene.
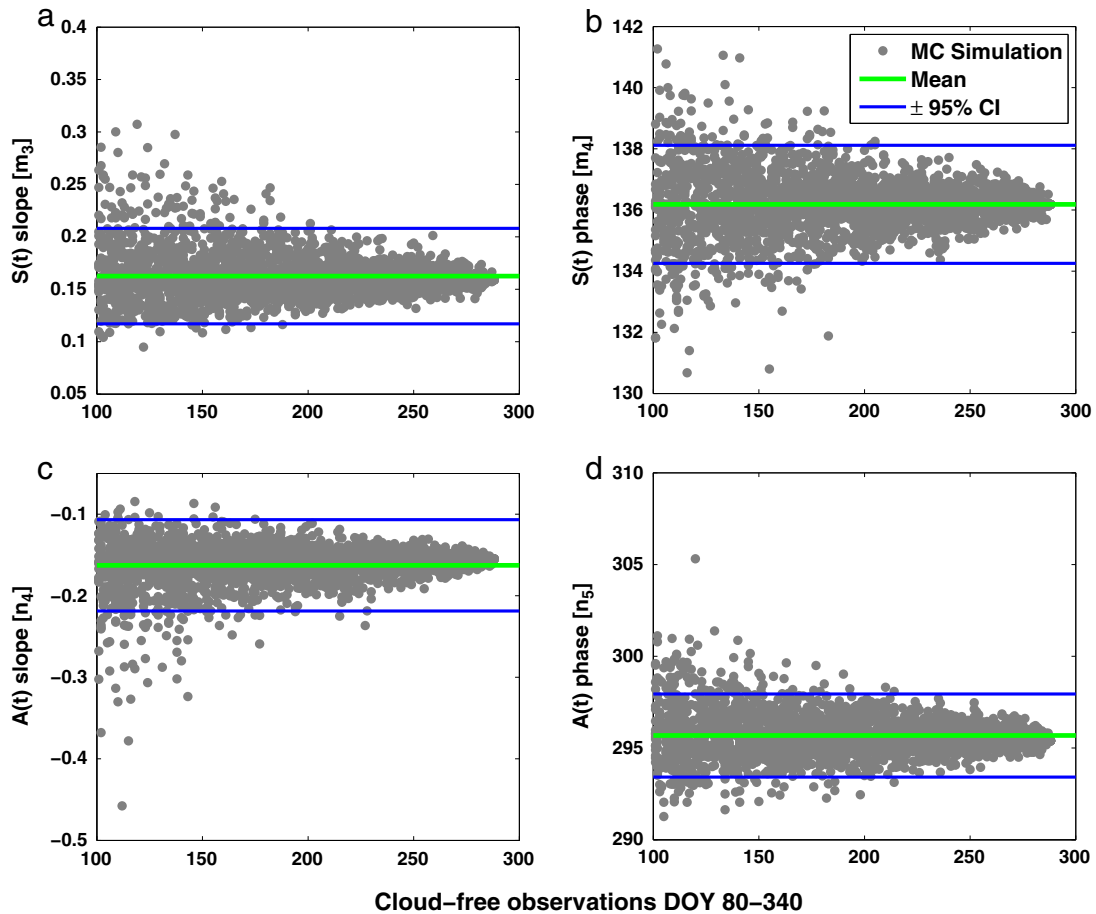
Fig. 7. Results from uncertainty analysis for slope and phase coefficients of logistic functions. Plots show the range of the slope (a, c) and phase coefficients (b, d) for spring (a, b) and autumn (c, d) logistic functions with respect to the number of available cloud-free observations between DOY 80-340. Green horizontal lines show the mean values for each coefficient and horizontal lines show 95% confidence intervals.

on comparison of results against field data collected at Harvard Forest, provides remarkably accurate results. Relative to coarser spatial resolution data sources such as MODIS and AVHRR, Landsat is able to resolve much greater fine-scale geographic variability in phenology. Landsat data therefore has substantial advantages in regions with heterogeneous land cover where topography, land use, and local microclimates can lead to substantial variation in phenology over relatively short spatial scales (Elmore et al., 2012; Fisher & Mustard, 2007). Equally important, the Landsat TM/ETM+ time series is now over 30 years long, which

makes it an excellent resource for studies of long-term phenological responses to climate change.

The 16-day revisit period provided by Landsat combined with missing data arising from cloud cover and the scan line corrector failure on the Landsat 7 ETM+ significantly reduces the frequency with which annual spring onset and autumn offset dates can be estimated — for the scene we considered here, it was possible to estimate these dates in only about one of every three years. One way to overcome this limitation is by spatially aggregating retrievals to provide statistical moments
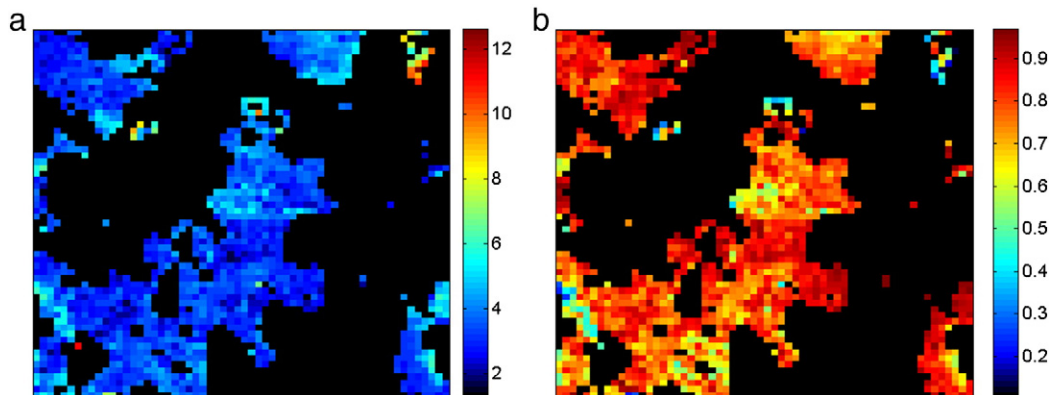

Fig. 8. (a) Root mean square error (days) between Landsat-derived spring onset date and the average date when the leaf length of deciduous tree species reached 25% of maximum across the 60×60 pixel window from Fig. 4; (b) R² for the same metrics. Note that only pixels classified as deciduous forest were included in the analysis.
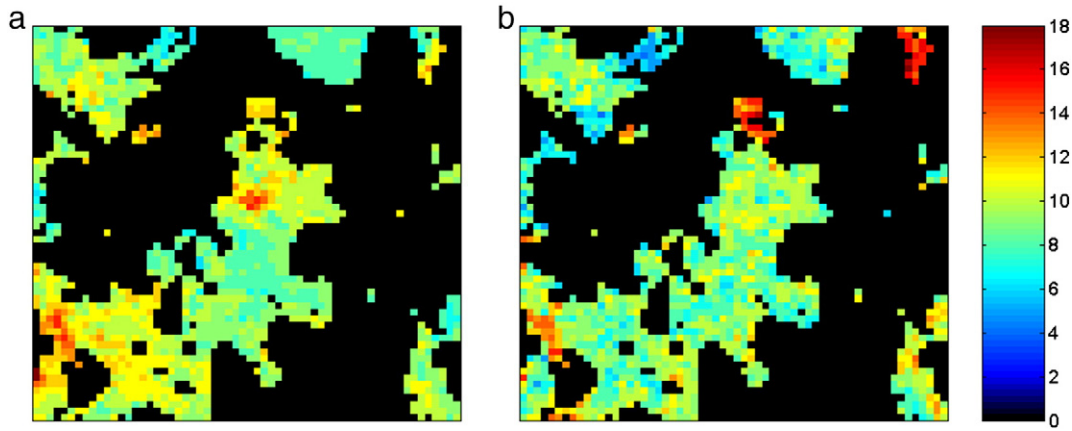
Fig. 9. Number of successful annual retrievals for (a) spring onset and (b) autumn offset derived from Landsat across the 60×60 pixel window in Fig. 4.

of onset and offset dates at coarser spatial resolution (e.g., the mean, median, and standard deviation in onset and offset dates at 1–5 km). However, devising the optimal method for doing this requires further research. Fig. 10, for example, presents boxplots for spring onset and autumn offset dates for the 60×60 pixel window centered over Harvard Forest shown in Figs. 8 and 9; even at this scale (~3 km²), significant gaps exist in the time series where no retrievals were made (e.g., 1982–1990 and 1996–1998 in spring; 1994–1998 in fall). Despite these gaps, it is striking to note that median spring onset and autumn offset dates in Fig. 10 vary by over 4 weeks.

Consistent with previous studies, spring onset and autumn offset dates estimated by our method reflect particular phenological metrics for the start and end of season (e.g., Hufkens et al., 2012a; Schwartz & Hanes, 2010). Specifically, the Landsat-based retrievals of spring onset dates at Harvard Forest provided unbiased and highly correlated estimates for the DOY when leaves reached 25% of their maximum size. However, depending on the application, different information related to phenology may be required (e.g., budburst date, which tends to occur 1–2 weeks earlier at Harvard Forest), and alternative remote sensing-based metrics may be more appropriate (e.g., Jonsson & Eklundh, 2002). Similarly, the timing and rate of senescence in autumn can vary by several weeks both among and within species (John O'Keefe, pers. comm.), making comparison of in-situ metrics with satellite-based measurements difficult, even at 30 m spatial resolution. Thus, more work is needed to develop flexible remote sensing-based metrics and methods that address the diverse needs of the ecological community.

Despite the encouraging results we show here, accurate characterization of uncertainty in remotely sensed measures of phenology remains an important challenge. For the method we describe in this paper, uncertainty in retrieved onset and offset dates is controlled by two main factors: (1) uncertainty in estimated slope and phase coefficients in Eqs. (1) and (2), and (2) noise in the EVI data. Our analysis suggests that uncertainty in estimates of the phase and slope coefficients translates into relatively modest uncertainties for annual spring onset and autumn offset dates. Our method also assumes that undetected clouds, cloud shadows, and other sources of noise that tend to reduce EVI value (thereby biasing estimates for spring onset and advancing autumn offset dates) are negligible. However, for the window shown in Figs. 8 and 9, the average rate of change in spring for the fitted spring logistic functions is 0.013 EVI/day. A decrease in EVI of 0.1 caused by clouds, shadows, or other sources of noise would therefore bias the estimated spring onset by 7 days (late). Our results do not show evidence of any significant bias, but high quality atmospheric correction and cloud screening is essential to the success of this method, and future efforts using this algorithm will need to assess this carefully.

The algorithm we present in this paper assumes that the rate of change of increase (spring) and decrease (fall) in EVI is consistent across years. However, recent studies have demonstrated that the rate of leaf growth can be much higher during anomalously warm springs than in more normal years (e.g., Barr et al., 2004; Hufkens et al., 2012b). To assess this, we fit logistic functions to annual time series of leaf length measurements for individual oak trees in the Harvard Forest field data set (not shown), and used the results to estimate uncertainty in the timing associated with 25% leaf length. Across all trees and all years, the standard deviation of the model slopes was ±0.08, which corresponds to an uncertainty of ±3.5 days for the DOY on which leaves achieve 25% their maximum length. This result supports our assumption that the rate of change in EVI (or leaf length) is relatively constant across years.

Finally, the assessment we present in this paper is limited to a temperate deciduous forest site in Southern New England. While the results we present are encouraging, future efforts are needed to more fully assess the method over a wider range of geographic and
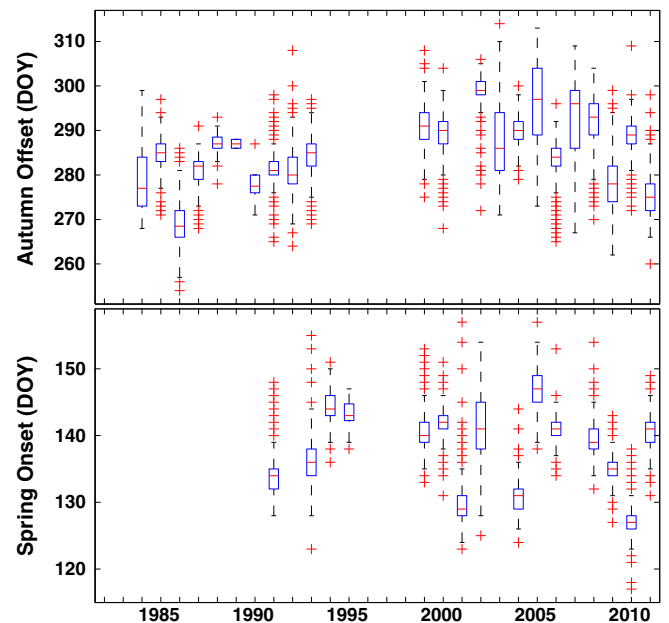

Fig. 10. Boxplots for autumn offset and spring onset dates across all deciduous forest pixels in the 60×60 Landsat pixel window in Fig. 4 from 1982 to 2011. The horizontal line in the center of each box is the median, the edges of each box are the 25th and 75th percentiles, and the whiskers extend to 1.5 times the interquartile range. Red points outside the whiskers are potential outliers.

ecological conditions. Areas located in the regions where adjacent Landsat scenes overlap are of particular interest, since twice as many data points are available for those areas. It may be possible to create gapless time series of spring onset and fall offset dates at these locations, supporting more extensive analysis of long-term phenological trends associated with climate variability and change. Evaluation is also needed across a broader range of ecosystems where phenology is strongly governed by air temperature (e.g., boreal forests) (Barr et al., 2004; Melaas et al., 2013), and more generally, in moisture-controlled ecosystems, where the coupling between climate and phenology is also strong, but where interannual variation in phenology can be significantly higher (>1 month; Williams et al., 1997).

5. Conclusions

Phenology is widely viewed to be an important diagnostic of climate change and is also a first-order control on biosphere–atmosphere interactions. As a result, remote sensing-based approaches for mapping and monitoring phenology have been the focus of substantial research over the past decade. To date, however, most efforts have focused on moderate spatial resolution data sources derived from sensors such as AVHRR, SPOT, MERIS and MODIS. These sensors provide frequent observations at global scale. However, substantial variation in phenology occurs below the spatial resolution of such instruments and cannot be retrieved from these data sources.

In this paper we describe and test a method to detect the timing of spring and autumn phenology for temperate deciduous forests using Landsat TM/ETM + data. Our results show that retrievals of spring and autumn transition dates correspond closely to phenological observations collected on the ground at Harvard Forest. Relative to coarser spatial resolution data sources that are commonly used to monitor phenology, Landsat is able to resolve much finer spatial detail and therefore captures geographic variability in phenology that is not observable from coarser spatial resolution sensors. Landsat-derived measurements of phenology therefore have advantages in regions with heterogeneous land cover, where the presence of evergreen forests can significantly complicate estimation of phenological metrics, or where other factors such as topography, land use, and microclimates create substantial variation in phenology over short spatial scales.

By providing information related to phenology at much finer spatial resolution, the 30 + year archive of Landsat data has the potential to significantly improve understanding of how climate controls phenology at interannual-to-decadal time scales and at regional-to-continental spatial scales. From a purely empirical perspective, long-term field observations related to phenology are quite rare, especially in North America. As a result, progress within the community focused on phenological theory and model development has been limited by available data. Recent initiatives prioritizing collection of ground or near-surface remote sensing based phenology data such as the PhenoCam (http://klima.sr.unh.edu/) and National Phenology Networks (www.usanpn.org/) are rapidly expanding available datasets (Betancourt et al., 2005; Richardson et al., 2009). In the near future, however, these efforts will not provide long-term observations that are urgently needed to improve understanding of how climate change affects the phenology of terrestrial ecosystems. The method we describe in this paper has the potential to substantially improve this data and knowledge gap. More effort is required to test this approach over a broader range of conditions, but at a minimum, the results presented here suggest that it should be possible to generate high-quality multi-decadal observations of phenology at 30 m spatial resolution over large areas of deciduous forest ecosystems.

Acknowledgments

References

Badeck, F. W., Bondeau, A., Bottcher, K., Doktor, D., Lucht, W., Schaber, J., et al. (2004). Responses of spring phenology to climate change. *New Phytologist, 162*(2), 295–309.

Badhwar, G. D. (1980). Crop emergence data determination from spectral data. *Photogrammetric Engineering and Remote Sensing, 46*, 369–377.

Barr, A. G., Black, T. A., Hogg, E. H., Kljun, N., Morgenstern, K., & Nesic, Z. (2004). Inter-annual variability in the leaf area index of a boreal aspen-hazelnut forest in relation to net ecosystem production. *Agricultural and Forest Meteorology, 126*, 237–255.

Betancourt, J. L., Schwartz, M. D., Breshears, D. D., Cayan, D. R., Dettinger, M. D., Inouye, D. W., et al. (2005). Implementing a U.S. National Phenology Network. *EOS Transactions AGU, 86*, 539–541.

Chuine, I., Morin, X., & Bugmann, H. (2010). Warming, photoperiods, and tree phenology. *Science, 329*(5989), 277–278.

Churkina, G., Schimel, D., Braswell, B. H., & Xiao, X. M. (2005). Spatial analysis of growing season length control over net ecosystem exchange. *Global Change Biology, 11*(10), 1777–1787.

Cleland, E. E., Chuine, I., Menzel, A., Mooney, H. A., & Schwartz, M. D. (2007). Shifting plant phenology in response to global change. *Trends in Ecology & Evolution, 22*(7), 357–365.

De Beurs, K. M., & Henebry, G. M. (2010). Spatio-temporal statistical methods for modelling land surface phenology. In Hudson, & Keatley (Eds.), *Phenological research: Methods for environmental and climate change analysis* (pp. 177–208).

Delpierre, N., Dufrene, E., Soudani, K., Ulrich, E., Cecchini, S., Boe, J., et al. (2009). Modelling interannual and spatial variability of leaf senescence for three deciduous tree species in France. *Agricultural and Forest Meteorology, 149*(6–7), 938–948.

Donohue, R. J., McVicar, T. R., & Roderick, M. L. (2009). Climate-related trends in Australian vegetation cover as inferred from satellite observations, 1981–2006. *Global Change Biology, 15*, 1025–1039.

Elmore, A. J., Guinn, S. M., Minsley, B. J., & Richardson, A. D. (2012). Landscape controls on the timing of spring, autumn, and growing season length in mid-Atlantic forests. *Global Change Biology, 18*(2), 656–674.

Fisher, J. I., & Mustard, J. F. (2007). Cross-scalar satellite phenology from ground, Landsat, and MODIS data. *Remote Sensing of Environment, 109*(3), 261–273.

Fisher, J. I., Mustard, J. F., & Vadeboncoeur, M. A. (2006). Green leaf phenology at Landsat resolution: Scaling from the field to the satellite. *Remote Sensing of Environment, 100*(2), 265–279.

Ganguly, S., Friedl, M. A., Tan, B., Zhang, X. Y., & Verma, M. (2010). Land surface phenology from MODIS: Characterization of the Collection 5 global land cover dynamics product. *Remote Sensing of Environment, 114*, 1805–1816.

Huete, A., Didan, K., Miura, T., Rodriguez, E. P., Gao, X., & Ferreira, L. G. (2002). Overview of the radiometric and biophysical performance of the MODIS vegetation indices. *Remote Sensing of Environment, 83*(1–2), 195–213.

Hufkens, K., Friedl, M. A., Keenan, T. F., Sonnentag, O., Bailey, A., O'Keefe, J., et al. (2012). Ecological impacts of a widespread frost event following early spring leaf-out. *Global Change Biology, 18*(7), 2365–2367.

Hufkens, K., Friedl, M., Sonnentag, O., Braswell, B. H., Milliman, T., & Richardson, A. D. (2012). Linking near-surface and satellite remote sensing measurements of deciduous broadleaf forest phenology. *Remote Sensing of Environment, 117*, 307–321.

Jonsson, P., & Eklundh, L. (2002). Seasonality extraction by function fitting to time-series of satellite sensor data. *IEEE Transactions on Geoscience and Remote Sensing, 40*, 1824–1832.

Levenberg, K. (1944). A method for the solution of certain problems in least squares. *Quarterly of Applied Mathematics, 2*, 164–168.

Liang, L. A., Schwartz, M. D., & Fei, S. L. (2011). Validating satellite phenology through intensive ground observation and landscape scaling in a mixed seasonal forest. *Remote Sensing of Environment, 115*, 143–157.

Masek, J. G., Huang, C. Q., Wolfe, R., Cohen, W., Hall, F., Kutler, J., et al. (2008). North American forest disturbance mapped from a decadal Landsat record. *Remote Sensing of Environment, 112*(6), 2914–2926.

Melaas, E. K., Richardson, A. D., Friedl, M. A., Dragoni, D., Gough, C. M., Herbst, M., Montagnani, L., & Moors, E. (2013). Using FLUXNET data to improve models of springtime vegetation activity onset in forest ecosystems. *Agricultural and Forest Meteorology, 171–172*, 46–56.

Moore, K. E., Fitzjarrald, D. R., Sakai, R. K., Goulden, M. L., Munger, J. W., & Wofsy, S. C. (1996). Seasonal variation in radiative and turbulent exchange at a deciduous forest in central Massachusetts. *Journal of Applied Meteorology, 35*(1), 122–134.

Morisette, J. T., Richardson, A. D., Knapp, A. K., Fisher, J. I., Graham, E. A., Abatzoglou, J., et al. (2009). Tracking the rhythm of the seasons in the face of global change: phenological research in the 21st century. *Frontiers in Ecology and the Environment, 7*, 253–260.

Moulin, S., Kergoat, L., Viovy, N., & Dedieu, G. (1997). Global-scale assessment of vegetation phenology using NOAA/AVHRR satellite measurements. *Journal of Climate, 10*(6), 1154–1170.

O'Keefe, J. (2000). *Phenology of woody species.* Harvard Forest Data Archive: HF003.

Reed, B. C., Brown, J. F., Vanderzee, D., Loveland, T. R., Merchant, J. W., & Ohlen, D. O. (1994). Measuring phenological variability from satellite imagery. *Journal of Vegetation Science, 5*, 703–714.

Richardson, A. D., Anderson, R. S., Arain, M. A., Barr, A. G., Bohrer, G., Chen, G., et al. (2012). Land surface models need better representation of vegetation phenology: Results

from the North American Carbon Program Site Synthesis. *Global Change Biology*, *18*, 566–584.

Richardson, A. D., Hollinger, D. Y., Dail, D. B., Lee, J. T., Munger, J. W., & O'Keefe, J. (2009). Influence of spring phenology on seasonal and annual carbon balance in two contrasting New England forests. *Tree Physiology*, *29*(3), 321–331.

Schwartz, M. D., Betancourt, J. L., & Weltzin, J. F. (2012). From Caprio's lilacs to the USA National Phenology Network. *Frontiers in Ecology and the Environment*, *10*, 324–327.

Schwartz, M. D., & Hanes, J. M. (2010). Intercomparing multiple measures of the onset of spring in eastern North America. *International Journal of Climatology*, *30*, 1614–1626.

Tan, B., Woodcock, C. E., Hu, J., Zhang, P., Ozdogan, M., Huang, D., et al. (2006). The impact of gridding artifacts on the local spatial properties of MODIS data: Implications for validation, compositing, and band-to-band registration across resolutions. *Remote Sensing of Environment*, *105*(2), 98–114.

Urbanski, S., Barford, C., Wofsy, S., Kucharik, C., Pyle, E., Budney, J., et al. (2007). Factors controlling CO_2 exchange on timescales from hourly to decadal at Harvard Forest. *Journal of Geophysical Research*, *112*, G02020. http://dx.doi.org/10.1029/2006/JG000293.

Vermote, E. F., El-Saleous, N., Justice, C. O., Kaufman, Y. J., Privette, J. L., Remer, L., et al. (1997). Atmospheric correction of visible to middle-infrared EOS-MODIS data over land surfaces: Background, operational algorithm and validation. *Journal of Geophysical Research-Atmospheres*, *102*(D14), 17131–17141.

Walker, J. J., de Beurs, K. M., Wynne, R. H., & Gao, F. (2012). Evaluation of Landsat and MODIS data fusion products for analysis of dryland forest phenology. *Remote Sensing of Environment*, *117*, 381–393.

White, M. A., de Beurs, K. M., Didan, K., Inouye, D. W., Richardson, A. D., Jensen, O. P., et al. (2009). Intercomparison, interpretation, and assessment of spring phenology in North America estimated from remote sensing for 1982–2006. *Global Change Biology*, *15*, 2335–2359.

White, M. A., Thornton, P. E., & Running, S. W. (1997). A continental phenology model for monitoring vegetation responses to interannual climatic variability. *Global Biogeochemical Cycles*, *11*, 217–234.

Williams, R. J., Myers, B. A., Muller, W. J., Duff, G. A., & Eamus, D. (1997). Leaf phenology of woody species in a North Australian tropical savanna. *Ecology*, *78*(8), 2542–2558.

Woodcock, C. E., Allen, R., Anderson, M., Belward, A., Bindschadler, R., Cohen, W., et al. (2008). Free access to Landsat imagery. *Science*, *320*(5879), 1011.

Xian, G., Homer, C., & Fry, J. (2009). Updating the 2001 National Land Cover Database land cover classification to 2006 by using Landsat imagery change detection methods. *Remote Sensing of Environment*, *113*, 1133–1147.

Zhang, X. Y., Friedl, M. A., Schaaf, C. B., Strahler, A. H., Hodges, J. C. F., Gao, F., et al. (2003). Monitoring vegetation phenology using MODIS. *Remote Sensing of Environment*, *84*(3), 471–475.

Zhu, X. L., Chen, J., Gao, F., Chen, X. H., & Masek, J. G. (2010). An enhanced spatial and temporal adaptive reflectance fusion model for complex heterogeneous regions. *Remote Sensing of Environment*, *114*(11), 2610–2623.

Zhu, Z., & Woodcock, C. E. (2012). Object-based cloud and cloud shadow detection in Landsat imagery. *Remote Sensing of Environment*, *118*, 83–94.